Simulation of a Schwarzschild Black Hole and its Accretion Disk

Maxime Soncin

The objective of this project is to computationally simulate the observation of a Schwarzschild black hole and its accretion disk. It is based on the theoretical study of the physical phenomena involved by such objects and their implementation in Python. The first part is devoted to the study of the deviation of photon trajectories by massive objects such as black holes and the numerical resolution of the appearance of these orbits. The second part presents the simulation of the observation of a black hole and its accretion disk, basing their representation on the radiation of a black body. The third part proposes a semi-quantitative study of the temperature distribution of the disk and its implementation in the simulation. Finally, the fourth part proposes the theoretical study and implementation of the different Doppler effects involved by these astrophysical objects.

1 Deviation of Photon Trajectories

1.1 Physical Phenomenon Studied and Tools of General Relativity

In Newtonian mechanics, two massive objects exert a force on each other according to the famous formula

$$\overrightarrow{f} = -G\frac{m_1 m_2}{r^2}\overrightarrow{u_r}$$

where m_1, m_2 are the masses of the objects and $\overrightarrow{u_r}$ is the unit vector collinear to the line joining them, and r is the distance separating them. This equation has long described the movements of celestial bodies accurately but has faced some anomalies. Indeed, for a photon of mass $m_{ph} = 0$, no gravitational force seems to deviate its trajectory. In practice, a deviation of light near massive objects is observed and is theoretically described using general relativity. In relativity, the space-time interval ds is defined such that ds^2 corresponds to the distance between two events. This quantity allows, in general relativity, to define the metric equation that describes the curvature of space-time around a considered object. In 1916, K. Schwarzschild proposed a metric describing the curvature of space-time around a spherically symmetric, non-rotating

object [1], which is written in spherical coordinates as:

$$ds^2 = -(1 - \frac{2GM}{c^2 r})c^2 dt^2 + (1 - \frac{2GM}{c^2 r})^{-1} dr^2 + r^2 d\theta^2 + r^2 \sin^2 \theta d\phi^2$$

We will admit the expression of this metric in this study. We will also use the system of geometric units in the following first part, where $G = c = 1$. The metric equation is rewritten as:

$$ds^2 = -(1 - \frac{2M}{r})dt^2 + (1 - \frac{2M}{r})^{-1} dr^2 + r^2 d\theta^2 + r^2 \sin^2 \theta d\phi^2$$

We are interested in the trajectory of photons in a space-time whose metric is that of Schwarzschild. The position of the photon in this space-time is given by a vector $x = (t, x, y, z)$ (in geometric units) or (t, r, θ, ϕ). The velocity of the photon is defined by the vector $u = \frac{dx}{d\lambda}$ with λ a variable introduced to parameterize the trajectory in curved space-time. The symmetries of this metric with respect to time t and rotation according to ϕ lead to the conservation of two quantities [2] that we will admit: Energy per unit rest mass:

$$e = (1 - \frac{2M}{r})\frac{dt}{d\lambda}$$

Angular momentum per unit mass:

$$l = r^2 \sin^2 \theta \frac{d\phi}{d\lambda}$$

The expression of the metric comes from a resolution of Einstein's field equations and the conservation of quantities from the invariance of the metric according to certain vectors called Killing vectors. They constitute the only admitted formulas that are not part of the MP program of this project.

1.2 Photon Deviation Equation

In general relativity, photons follow light-like world lines, i.e., such that $ds^2 = 0$. By dividing by $d\lambda^2$, the metric is rewritten as:

$$0 = -(1 - \frac{2M}{r})\frac{dt^2}{d\lambda^2} + (1 - \frac{2M}{r})^{-1}\frac{dr^2}{d\lambda^2} + r^2\frac{d\theta^2}{d\lambda^2} + r^2 \sin^2 \theta \frac{d\phi^2}{d\lambda^2}$$

We seek to find a numerically solvable equation allowing us to find the complete trajectory of the photon. By symmetry with respect to θ, we set $\theta = \frac{\pi}{2}$ and consider $d\theta = 0$. The expression becomes:

$$-(1 - \frac{2M}{r})(\frac{dt}{d\lambda})^2 + (1 - \frac{2M}{r})^{-1}(\frac{dr}{d\lambda})^2 + r^2(\frac{d\phi}{d\lambda})^2 = 0$$

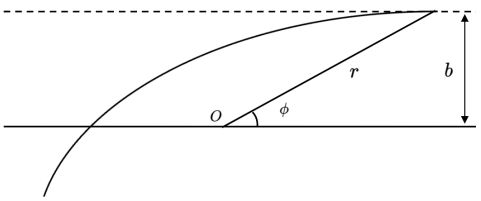

Fig. 1 Schematic of photon deviation and definition of the impact parameter b

By replacing the expressions for $\frac{dt}{d\lambda}$ and $\frac{d\phi}{d\lambda}$ using the conservation equations for e and l, we get:

$$-(1-\frac{2M}{r})^{-1}e^2+(1-\frac{2M}{r})^{-1}(\frac{dr}{d\lambda})^2+\frac{l^2}{r^2}=0$$

By dividing by l^2 and multiplying by $(1-\frac{2M}{r})$,

$$-\frac{e^2}{l^2}+\frac{1}{l^2}(\frac{dr}{d\lambda})^2+\frac{1}{r^2}(1-\frac{2M}{r})=0$$

Or

$$\frac{1}{l^2}(\frac{dr}{d\lambda})^2=\frac{e^2}{l^2}-\frac{1}{r^2}(1-\frac{2M}{r})$$

Taking the square root of this expression and considering only the positive solution,

$$\frac{1}{l}\frac{dr}{d\lambda}=(\frac{e^2}{l^2}-\frac{1}{r^2}(1-\frac{2M}{r}))^{\frac{1}{2}}$$

And since $l=r^2\frac{d\phi}{d\lambda}$,

$$\frac{dr}{d\phi}=r^2(\frac{e^2}{l^2}-\frac{1}{r^2}(1-\frac{2M}{r}))^{\frac{1}{2}}$$

Now, as r tends to infinity, $\left|\frac{l}{e}\right|\sim r^2\frac{d\phi}{dt}=r^2\frac{d\phi}{dr}\frac{dr}{dt}$. And, far from the black hole, $\frac{dr}{dt}\sim 1$ (in geometric units) and, as shown in the diagram, $b=r\sin\phi$, so $\phi\sim\frac{b}{r}$ and thus

$$\left|\frac{l}{e}\right|\sim r^2\frac{d\phi}{dr}\sim r^2\frac{d(\frac{b}{r})}{dr}=b$$

We finally obtain:

$$\frac{dr}{d\phi}=r^2(\frac{1}{b^2}-\frac{1}{r^2}(1-\frac{2M}{r}))^{\frac{1}{2}} \tag{1}$$

1.3 Numerical Approximation of Photon Trajectories

The numerical resolution of equation 1 allows us to obtain the polar trajectory $(r(\phi),\phi)$ of a given photon. We implement the numerical resolution scheme using a first-order Euler method, which provides intuitive and sufficiently fast results for the rest of the implementation. By fixing an initial angle ϕ_0, we obtain the graphical representation of the trajectories. The black hole horizon is represented by a black

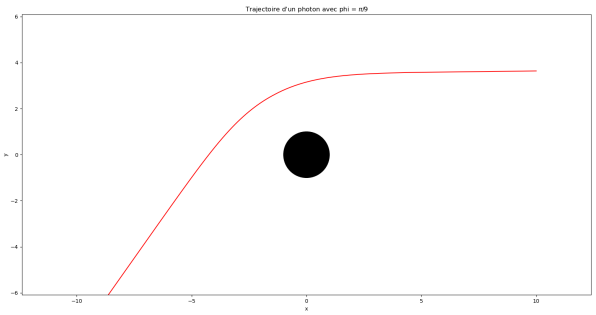

Fig. 2 Simulation of photon deviation with an initial angle $\phi_0 = \frac{\pi}{9}$

spot of radius $R_s = 2M$. Comments: The obtained deviation is consistent with the expected result illustrated in figure 1: the black hole "attracts" the photon (even though it has no mass), so the trajectory is centripetal. We represent in figure 3 different interesting trajectories, notably showing a limiting impact parameter b_c for $b_c = x_0 \tan\left(\frac{\pi}{12.35933}\right) \sim 2.598$ a.u. Near this value b_c, the photon can make a U-turn,

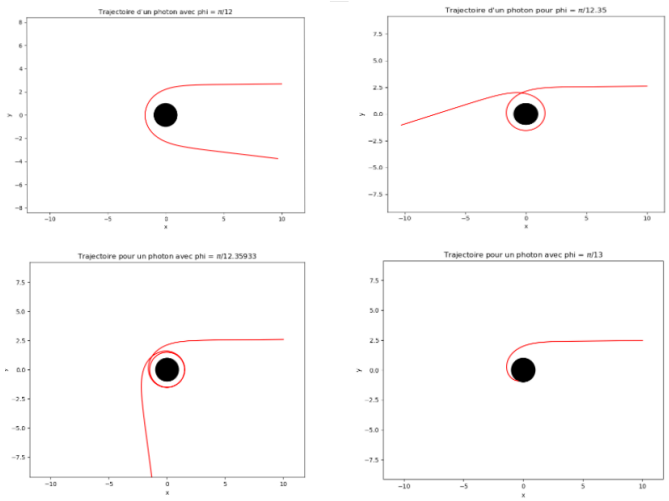

Fig. 3 Simulation of photon deviation with initial angles $\phi_0 = \frac{\pi}{12}, \frac{\pi}{12.35}, \frac{\pi}{12.35933}, \frac{\pi}{13}$

one or even several orbits around the black hole before escaping. This phenomenon was impossible in Newtonian theory. It can be shown that the theoretical value of b_c is $b_c = \sqrt{27}M \sim 2.598$ a.u. The value found by our simulation is therefore very close to the theoretical value (relative error of the order of 10^{-7}). We can then simultaneously simulate the trajectory of any number n of photons to better represent the influence of the choice of the initial angle on the obtained deviation.

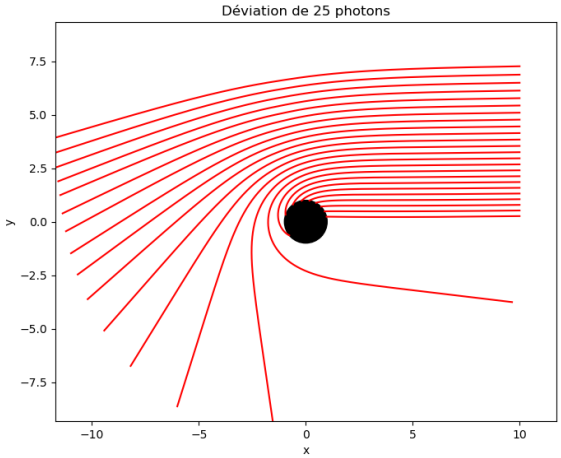

Fig. 4 Simulation of the deviation of 25 photons with initial angles varying from $\phi_0 = 0$ to $\phi_0 = \frac{\pi}{5}$

1.4 3D Representation by Raytracing

To simulate the real observation of a black hole and its accretion disk, it is possible to use a "raytracing" method to represent them. The goal being to obtain an image of these astrophysical objects, the principle of raytracing is to associate each pixel of this image with a photon and to "send" them in the direction of the black hole and the disk, then to associate a color with them depending on the zone of the object with which they collided. This method amounts to tracing the photons back in time from the camera's objective to determine by which objects they were emitted and to associate the appropriate color with them. We then add an accretion disk to our model. In this part, we will arbitrarily assign the color light gray to photons emitted by the accretion disk and received by the camera, and represent in black those that have been absorbed by the black hole horizon. The thickness, radius, and color of the disk are therefore chosen arbitrarily in this part. We then represent in figure 5 the simulated observation obtained by raytracing with a resolution of 128×128 pixel-photons for different disk thickness values e, in arbitrary units. The results obtained resemble the

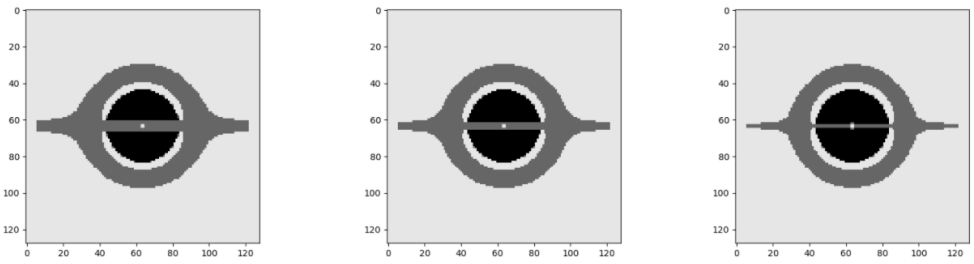

Fig. 5 Simulation of the observation of the black hole and its disk for different disk thicknesses $e = 0.7, 0.5, 0.3$ in arbitrary units

classic representation of these objects. However, we can note a simulation aberration at the center of the figure, which is due to the choice of the resolution step. This aberration will be corrected in part 4. We can then increase the resolution of the image to obtain more satisfactory results. Figure 6 presents a simulation with a resolution of 512×512 pixel-photons for a disk thickness $e = 0.3$. The obtained simulations

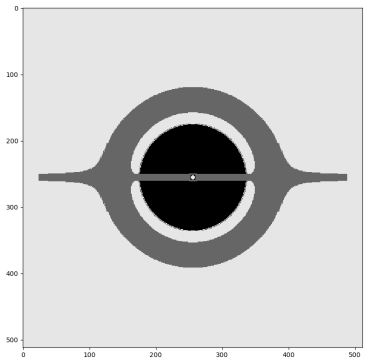

Fig. 6 Simulation of the observation of the black hole and its disk for a disk thickness $e = 0.3$ in arbitrary units with better resolution

seem to correspond to the expected results. However, many parameters were chosen arbitrarily: the radius of the disk, its thickness, and its color. The following parts aim to address this by proposing more quantitative models for the radius and color of the accretion disk.

2 Realistic Representation of the Disk Color

2.1 The Disk as a Black Body

A reasonable idea to give a realistic color to the previously represented accretion disk is to consider it as a black body. Thus, if we assume its temperature distribution is known, by approximating the disk as a black body, we can convert its theoretical radiation into RGB values and thus into an image. We will therefore assume in the following that the disk radiates as a black body, i.e., that its radiation follows Planck's law [3]:

$$u_\lambda(\lambda, T) = \frac{8\pi hc}{\lambda^5} \frac{1}{e^{\frac{hc}{k_B T \lambda}} - 1}$$

With $u_\lambda(\lambda, T)$ spectral energy density: it is the energy radiated per unit volume of black body in the interval $[\lambda, \lambda + d\lambda[$. This result is not part of the MP program but

is accessible with the tools introduced by the latter. We propose to demonstrate it in

what follows. We consider a cubic cavity of side L whose walls are perfectly reflective. By making a hole of size small compared to L^2, this radiating cavity appears as a black body. Planck postulates in his demonstration that the energy emitted by the black

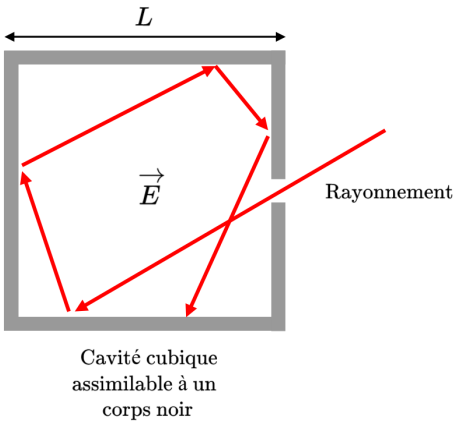

Fig. 7 Schematic of the cubic cavity whose radiation is assimilated to that of a black body

body is quantized. The energy associated with a mode of index n of the electromagnetic waves present in the cavity is that of a harmonic oscillator and is written:

$$U_n(m) = m\hbar\omega_n$$

with $(n, m) \in \mathbb{N}^2$ The probability that a mode n has an energy of $U_n(m)$ is then written:

$$p_{n,m} = \frac{1}{Z_n} \exp\left(\frac{-m\hbar\omega_n}{k_B T}\right)$$

with $Z_n = \frac{1}{\sum_{m=0}^{+\infty} \exp\left(\frac{-m\hbar\omega_n}{k_B T}\right)}$ The wave radiated by the black body in a given mode n can have two distinct polarizations, so the energy state associated with each mode n is doubly degenerate. We deduce that for this mode, the average energy is written as

$$< U_n >= \sum_{m=0}^{+\infty} 2U_n(m)p_{n,m} = 2\hbar\omega_n \frac{\sum_{m=0}^{+\infty} m \exp\left(\frac{-m\hbar\omega_n}{k_B T}\right)}{\sum_{m=0}^{+\infty} \exp\left(\frac{-m\hbar\omega_n}{k_B T}\right)}$$

We simplify the expression of $< U_n >$ by introducing the variable t such that:

$$< U_n >= 2\hbar\omega_n \frac{\partial}{\partial t} - \ln\left(\sum_{m=0}^{+\infty} e^{-mt}\right)\Bigg|_{t=\frac{\hbar\omega_n}{k_B T}}$$

Hence

$$< U_n >= 2\hbar\omega_n \frac{\partial}{\partial t}(-\ln\left(\frac{1}{1-e^{-t}}\right))\Big|_{t=\frac{\hbar\omega_n}{k_B T}} = 2\hbar\omega_n \frac{\partial}{\partial t}\ln\left(1-e^{-t}\right)\Big|_{t=\frac{\hbar\omega_n}{k_B T}}$$

We finally obtain:

$$< U_n >= 2\hbar\omega_n \frac{e^{-\frac{\hbar\omega_n}{k_B T}}}{1-e^{-\frac{\hbar\omega_n}{k_B T}}} = \frac{2\hbar\omega_n}{e^{\frac{\hbar\omega_n}{k_B T}}-1}$$

We can then note the spectral energy density, i.e., the energy per unit volume of the black body and per unit wavelength:

$$u_\lambda(\lambda, T) = G(\lambda)\frac{< U_n >}{L^3}$$

With $G(\lambda)$ the number of modes per unit wavelength. We seek to determine this quantity. For this, we determine $G(k)$, the number of modes per unit wave vector. The boundary conditions imposed by the reflecting mirrors imply a quantization of the modes of the electromagnetic waves present inside the cavity. The wave vector $\overrightarrow{k_n}$ associated with mode n is written as:

$$\overrightarrow{k_n} = 2\pi(\frac{n_x}{L}\overrightarrow{u_x} + \frac{n_y}{L}\overrightarrow{u_y} + \frac{n_z}{L}\overrightarrow{u_z})$$

In the space of wave vectors, each mode n therefore occupies a "volume" which is written:

$$\delta^3 k = \frac{2\pi}{L} \times \frac{2\pi}{L} \times \frac{2\pi}{L} = \frac{8\pi^3}{L^3}$$

When k varies from k to $k + dk$, the number of modes per unit volume is therefore written:

$$n(k) = \frac{\text{infinitesimal volume between } k \text{ and } k+dk}{\text{volume occupied by a mode}} = \frac{4\pi k^2 dk}{\delta^3 k} = \frac{L^3 k^2 dk}{2\pi^2}$$

Since $k = \frac{2\pi}{\lambda}$, and taking $n(\lambda) > 0$,

$$n(\lambda) = \frac{L^3 4\pi^2}{2\pi^2\lambda^2} \times 2\pi\frac{d\lambda}{\lambda^2} = \frac{4\pi L^3}{\lambda^4}d\lambda$$

Hence, $G(\lambda) = \frac{4\pi L^3}{\lambda^4}$ By reinjecting into the expression, and since $\omega_n = \frac{2\pi c}{\lambda}$ and $\hbar = \frac{h}{2\pi}$, we get:

$$u_\lambda(\lambda, T) = \frac{4\pi L^3}{\lambda^4} \times \frac{2hc}{\lambda} \times \frac{1}{L^3} \times \frac{1}{e^{\frac{\hbar c}{k_B T\lambda}}-1}$$

Finally:

$$u_\lambda(\lambda, T) = \frac{8\pi hc}{\lambda^5}\frac{1}{e^{\frac{\hbar c}{k_B T\lambda}}-1} \tag{2}$$

Assuming isotropic radiation throughout the space of the black body, between t and $t + dt$, all the radiated power is found in a sphere of radius cdt. The spectral power per unit solid angle is therefore written as:

$$L_\lambda(\lambda, T)dt = \underbrace{\frac{cdt}{4\pi}}_{\text{per unit solid angle}} \qquad u_\lambda(\lambda, T) = \frac{2hc^2}{\lambda^5} \frac{dt}{e^{\frac{\hbar c}{k_B T \lambda}} - 1}$$

In practice, for numerical implementation, we use the spectral radiant exitance, i.e., the spectral power radiated per unit area of the black body. It is defined here by:

$$M_\lambda(\lambda, T) = \int_{\text{half-space}} L_\lambda(\lambda, T)\overrightarrow{u_z}.\overrightarrow{\Omega}\, d\Omega = \int_{\text{half-space}} L_\lambda(\lambda, T)\cos\theta d\Omega$$

Since the radiation is assumed to be isotropic, we deduce that:

$$M_\lambda(\lambda, T) = L_\lambda(\lambda, T) \int_{\phi=0}^{2\pi} \int_{\theta=0}^{\frac{\pi}{2}} \cos\theta \sin\theta d\theta d\phi = \pi L_\lambda(\lambda, T)$$

Hence:

$$M_\lambda(\lambda, T) = \frac{2\pi hc^2}{\lambda^5} \frac{1}{e^{\frac{\hbar c}{k_B T \lambda}} - 1}$$

2.2 Numerical Representation of the Emitted Spectrum

We then numerically plot the spectral exitance as a function of wavelength for black bodies at different temperatures: we thus retrieve the classic curve of black body radiation. From then on, we associate a color in the RGB computer system with an object of assumed known temperature by summing the energy contributions in the visible domain and converting them into red, green, and blue channels. We plot in figure 9 the color associated as a function of the temperature of the considered black body. This representation of color as a function of temperature is then implemented in the raytracing program and allows us to give the accretion disk a characteristic color of a given temperature. We thus represent in figure 10 the simulation of the observation of a black hole for different temperatures. Note that for the movie *Interstellar*, Kip

Thorne and his team used this uniform black body radiation model to create the accretion disk of the black hole Gargantua [4]. The temperature used was $4500K$, as shown in figure 10, top right. We find a similar color to that of the film.

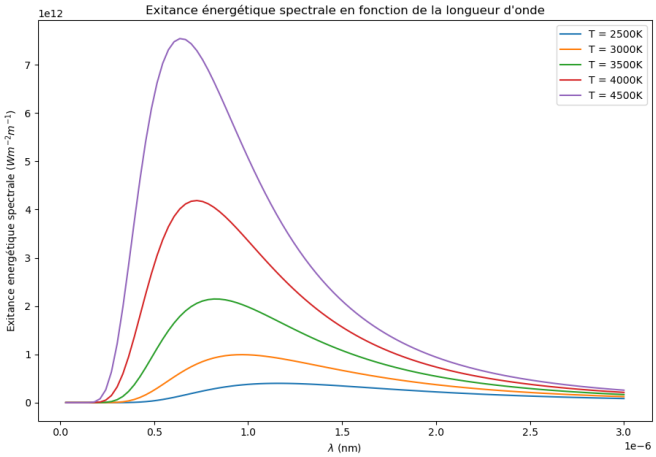

Fig. 8 Spectral radiant exitance as a function of wavelength for $T = 2500K, 3000K, 3500K, 4000K, 4500K$

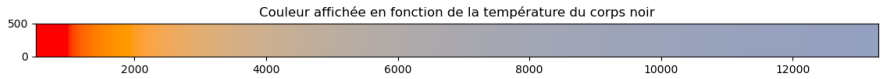

Fig. 9 Gradient of the color associated with the radiation of a black body as a function of temperature for $T \in [500K, 13300K]$

2.3 Affine Variation of Temperature with Radius

In reality, the speed of the matter composing the accretion disk depends on the distance from the center of the black hole. A particle closer to the horizon with a stable orbit will have a higher speed and thus a higher temperature than a particle located at a greater distance. We model this phenomenon initially by a temperature that depends affinely on the distance from the center of the black hole. This model is purely qualitative and the implementation of a more quantitative model is the subject of part 3. For this qualitative model, we then simulate the observation of the black hole and its accretion disk having a temperature distribution law as follows:

$$T(r) = T_0 - \Gamma r$$

Here, we arbitrarily choose $T_0 = 4500K$ and $\Gamma = 350K.ud^{-1}$ with ud the arbitrary distance unit chosen for the simulation. The background color is chosen to be black for visibility. The result of this simulation on a 1024×1024 pixel grid is presented in figure 11. Comment: By increasing the number of pixels in the image, we observe that the black hole horizon seems to be surrounded by a halo of photons that reached the observer, highlighted in figure 12. This phenomenon is observed because, near the horizon, the trajectory of photons is extremely deviated so that a photon emitted by the disk and passing close to the horizon can land in the observer's eye.

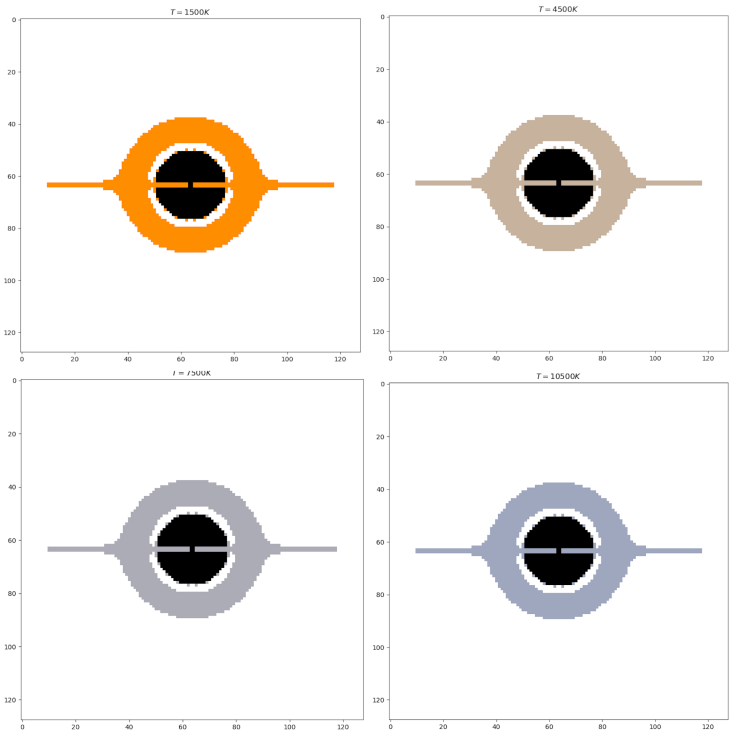

Fig. 10 Simulation of the observation of the black hole and its disk by giving the disk a uniform temperature with (from top to bottom and right to left) $T = 1500K, 4500K, 7500K, 10500K$

3 Temperature Distribution of the Disk

3.1 Dimensional Approximation of the Temperature Distribution

The objective of this part is to approach an expression for the temperature distribution within the disk. Obtaining an analytical solution for this temperature in a general framework is still today the subject of much research. The complete resolution, even in the least complex models, involves advanced fluid mechanics concepts that are beyond the scope of the MP program. We propose in what follows to retrieve the radial dependence of the temperature thanks to a dimensional reasoning. The results obtained will therefore be defined up to a multiplicative constant. We will assume in

what follows, as a first approximation, that the particles inside the disk are in circular orbits that follow Kepler's laws. By applying the fundamental principle of dynamics in the Frenet frame to one of these particles in the reference frame of the black hole assumed to be Galilean, we get:

$$\frac{v_\phi^2}{r} = \frac{GM}{r^2}$$

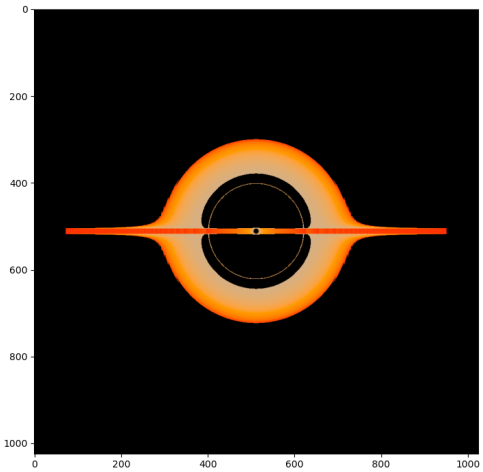

Fig. 11 Simulation of observation with affine variation of temperature as a function of r with $T_0 = 4500K$ and $\Gamma = 350K.ud^{-1}$

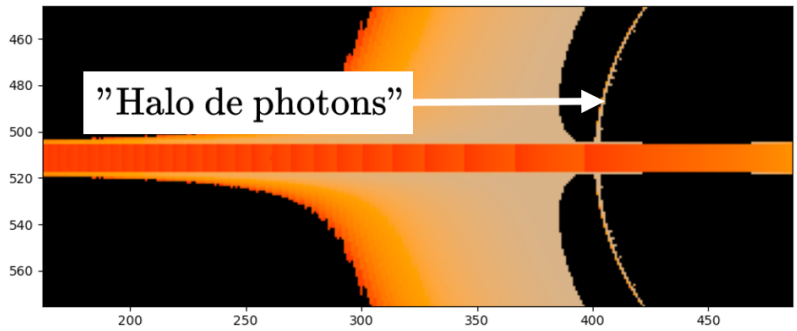

Fig. 12 Observation of the "photon halo" around the black hole horizon

Hence:

$$v_\phi = \sqrt{\frac{GM}{r}}$$

And since $\omega = \frac{2\pi}{T_{orbit}} = \frac{2\pi}{2\pi r} v_\phi$,

$$\omega = \sqrt{\frac{GM}{r^3}}$$

3.2 Stefan-Boltzmann Law

By assimilating the disk to a black body as before, the surface power emitted, i.e., the total radiant exitance, is written as:

$$I_{tot} = \int_{\lambda=0}^{+\infty} M_\lambda d\lambda = \int_{\lambda=0}^{+\infty} \frac{2\pi hc^2}{\lambda^5} \frac{d\lambda}{e^{\frac{\hbar c}{k_B T \lambda}} - 1}$$

By making the change of variables: $x = \frac{hc}{\lambda k_B T}$, i.e., $d\lambda = -\frac{1}{x^2}\frac{hc}{k_B T}dx$, we get

$$I_{tot} = \frac{2\pi h^2 c^3}{k_B T(\frac{hc}{k_B T})^5}\int_{x=0}^{+\infty}\frac{x^3}{e^x-1}dx = \underbrace{(\frac{2\pi k_B^4}{h^3c^2}\int_{x=0}^{+\infty}\frac{x^3}{e^x-1}dx)}_{=\sigma\approx 5.67\times 10^{-8} W.m^{-2}.K^{-4}}\ T^4$$

We deduce the Stefan-Boltzmann law:

$$I_{tot} = \sigma T^4$$

3.3 Dimensional Reasoning

We model the accretion disk again as a black body that satisfies this law. We seek to express the temperature T of the disk. By cylindrical symmetry (the black hole is not rotating so it is well verified) and assuming the disk is thin enough to consider that the temperature is the same throughout the thickness of the disk, the temperature depends only on the distance from the center r. We seek an expression for I_{tot} as a function of the parameters describing the accretion disk. One of the main parameters is the accretion rate $\dot{M} = \frac{dM}{dt}$, i.e., the mass accreted into the black hole per unit time. Moreover, the surface power emitted also seems to depend on the speed of the particles at fixed r (different speeds cause friction and are converted into thermal energy by radiation). It therefore seems judicious to look for an expression for I_{tot} of the form

$$I_{tot} \propto \dot{M}^a \omega^b$$

with $(a, b) \in \mathbb{Z}^2$ to be found. I_{tot} is in $W.m^{-2}$ so in $kg.s^{-3}$. Since ω is in s^{-1} and $\dot{M}$ in $kg.s^{-1}$, we get: $b = 1$ and $a = 2$. Hence:

$$I_{tot} = \sigma T^4 \propto \dot{M}\omega^2$$

But since $\omega \propto r^{-3/2}$, we deduce that

$$T(r) \propto r^{-\frac{3}{4}}$$

This semi-quantitative reasoning does not take into account the complexity of the phenomena involved: in more elaborate models, the gas composing the disk is in turbulent flow and the magnetic fields present complicate the resolution. In 1973, N. I. Shakura and R. A. Sunyaev proposed a model called the α disk [5] which models these phenomena by introducing a viscosity $\nu = \alpha c_s^2 H$ with H characteristic height of the disk, c_s the speed of sound in the disk and α coefficient in $[0, 1]$ which accounts for the phenomena of magnetism and turbulence involved. For a thin, optically thick disk and at a great distance from the center of the disk ($r \gg R_s$ with R_s Schwarzschild radius), the Shakura and Sunyaev model proposes a temperature distribution of the form

$$T_{\text{alpha disk}}(r) \propto (\alpha M)^{-\frac{1}{4}} r^{-\frac{3}{4}}$$

Thus, with Newtonian analogies and dimensional reasoning, we approach the solutions of more elaborate models. We will use this dependence in $r^{-\frac{3}{4}}$ for future simulations.

3.4 Simulation with the $r^{-\frac{3}{4}}$ Dependence

We thus model the temperature according to a law of the form $T(r) = Kr^{-\frac{3}{4}}$. The constant K remains to be chosen by defining a boundary condition for the temperature at the last stable circular orbit at $r = 3R_s$ (the expression for the radius of this orbit is shown in the appendix). Figure 13 presents four observation simulations for different limit temperatures. The temperature distribution thus obtained provides

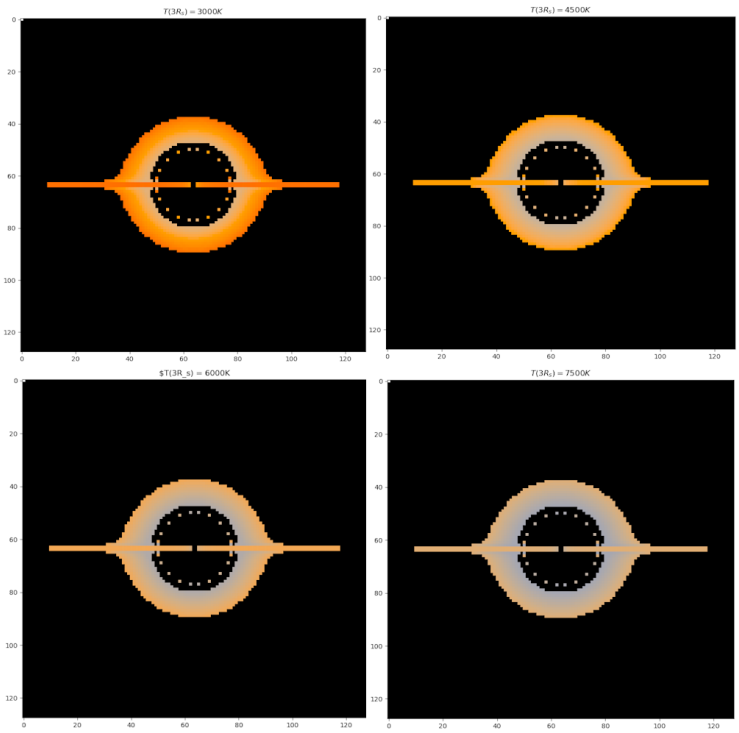

Fig. 13 Simulation of the observation of the black hole and its disk by giving the disk a temperature dependent on $r^{-\frac{3}{4}}$ with a boundary condition (from top to bottom and right to left) $T = 3000K, 4500K, 6000K, 7500K$ on a grid of resolution 128×128 pixels

different results compared to those obtained by the first qualitative law of an affine temperature in r. Although the choice of the limit temperature remains arbitrary, the obtained modeling has gained in realism compared to the old model. We will impose in the following the boundary condition $T(3R_s) \sim 3000K$. By using this law for the temperature for an image of 2048×2048 pixels, we obtain the simulated observation in figure 14. Although the model adopted in this part is based on dimensional rea-

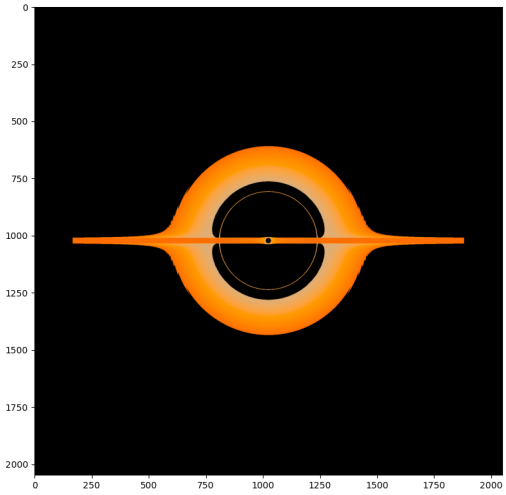

Fig. 14 Simulation of the observation of the black hole and its accretion disk for a limit temperature $T(3R_s) \sim 3000K$ on an image of 2048×2048 pixels

soning, it has allowed us to approach a more realistic modeling of an accretion disk and thus to obtain a better numerical representation of it.

4 Implementation of Doppler Effects

4.1 Classical Doppler-Fizeau Effect

In this last part, we are interested in the study and implementation in the simulation of the different Doppler effects involved by the black hole and its disk. The first effect studied is analogous to the Doppler effect relative to acoustic waves but it affects the frequency of electromagnetic waves. The matter constituting the accretion disk rotates around it at speeds that can approach that of light. Indeed, since $v_{\text{orbit}} = \sqrt{\frac{GM}{r}}$, the speed of a particle at the last stable orbit is written:

$$v_{ISCO} = \sqrt{\frac{GM}{3 \times \frac{2GM}{c^2}}} = \frac{c}{\sqrt{6}} \sim 1.2 \times 10^8 m.s^{-1}$$

The speeds involved are therefore relativistic and the wavelength shift must take this into account. The effect involved is therefore the Doppler-Fizeau effect [6] for relativistic speeds. We assume that a monochromatic plane light wave is emitted from the disk. It is written as:

$$\phi(\overrightarrow{r}, t) = A \exp(i(k_x x + k_y y + k_z z - \omega t))$$

With $\omega = \frac{2\pi c}{\lambda}$ and $\overrightarrow{k}$ the associated wave vector. In special relativity, the scalar product between four-vectors **A** and **B** is defined by:

$$\mathbf{A}.\mathbf{B} = -A^t B^t + A^x B^x + A^y B^y + A^z B^z$$

Thus, the quantity $k_x x + k_y y + k_z z - \omega t$ can be interpreted as the opposite of the scalar product of the two four-vectors: $\mathbf{x} = (ct, x, y, z)$ and $\mathbf{k} = (\frac{\omega}{c}, k_x, k_y, k_z)$:

$$\mathbf{x}.\mathbf{k} = -\omega t + k_x x + k_y y + k_z z$$

We associate with the observer and the particle emitting this light wave reference frames denoted $\mathcal{R}$ and $\mathcal{R}'$ respectively. We then denote $(\frac{\omega}{c}, k_x, k_y, k_z)$ and $(\frac{\omega'}{c}, k'_x, k'_y, k'_z)$ the expression of the four-vector **k** in each of these reference frames. We choose the x axis for the direction between the observer and the center of the black hole as indicated in the diagram below. Thus, the Lorentz transformation between the

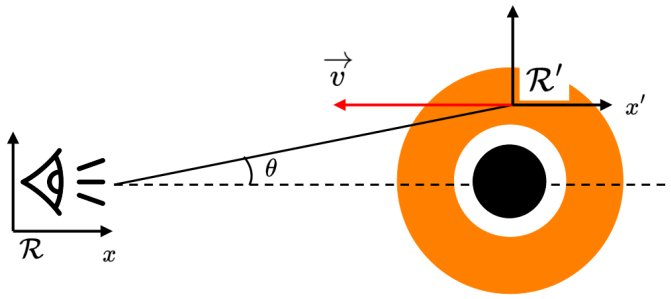

Fig. 15 Doppler-Fizeau effect diagram (top view)

reference frame of the emission of the wave $\mathcal{R}'$ and the reception reference frame $\mathcal{R}$ is written as:

$$\begin{pmatrix} \omega/c \\ k_x \\ k_y \\ k_z \end{pmatrix} = \begin{pmatrix} \gamma & -\gamma\beta & 0 & 0 \\ -\gamma\beta & \gamma & 0 & 0 \\ 0 & 0 & 1 & 0 \\ 0 & 0 & 0 & 1 \end{pmatrix} \begin{pmatrix} \omega'/c \\ k'_x \\ k'_y \\ k'_z \end{pmatrix}$$

With $\beta = \frac{v}{c}$ and $\gamma = \frac{1}{\sqrt{1-\beta^2}}$ The demonstration of the expression of this Lorentz transformation for a four-vector is done in the appendix. We then obtain, noting that $k'_x = -k' \cos\theta$ with θ defined as in figure 15:

$$\frac{\omega}{c} = \gamma(\frac{\omega'}{c} + \beta k' \cos\theta)$$

And since $k' = \frac{2\pi}{\lambda_{emitted}}$ and $\omega' = \frac{2\pi c}{\lambda_{emitted}}$

$$\frac{2\pi}{\lambda_{received}} = \frac{2\pi\gamma}{\lambda_{emitted}}(1 + \beta\cos\theta)$$

Hence

$$\lambda_{received} = \frac{\lambda_{emitted}}{\gamma(1 + \beta\cos\theta)}$$

Now, assuming that the observation of the disk is made at a very large distance compared to its size, we can estimate, as a first approximation, that $\theta \sim 0$. So that the previous expression is rewritten as:

$$\lambda_{received} = \lambda_{emitted}\frac{\sqrt{(1+\beta)(1-\beta)}}{(1+\beta)}$$

That is:

$$\lambda_{received} = \lambda_{emitted}\sqrt{\frac{1-\beta}{1+\beta}}$$

This is the formula for the longitudinal Doppler-Fizeau effect.

4.2 Simulation with the Addition of the Doppler-Fizeau Effect

We implement this effect in the simulation by giving as value for v appearing in $\beta = \frac{v}{c}$, the radial velocity with respect to the x axis, i.e., the apparent velocity of a particle of the disk in the eyes of the observer. Denoting ϕ the angle between the center of the black hole and the particle at a time t, this velocity is therefore given by

$$v_r = v_{orbit}\cos\phi$$

We then simulate the observation of the black hole and its disk on an image of resolution 2048×2048 pixels by assigning to v_{orbit} the numerical value of the Keplerian orbital velocity in geometric units: $v_{orbit} = \sqrt{\frac{M}{r}}$. The result of the simulation is presented in figures 16 and 17. Comments: The implemented Doppler effect slightly modifies the color of the disk in the regions where the relative velocities with respect to the observer are highest. The result then seems consistent: the light emitted by the matter moving towards the observer is shifted towards the blue while that moving in the opposite direction is shifted towards the red (redshift). The redshift of the light emitted by an object moving away from the observer is observed in practice for distant galaxies, moving away from Earth at high speeds. We find a similar effect here.

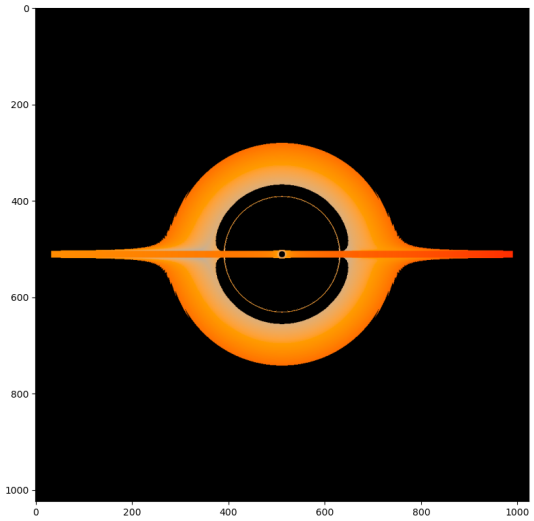

Fig. 16 Simulation of the observation of the black hole and its accretion disk with the implementation of the Doppler-Fizeau effect

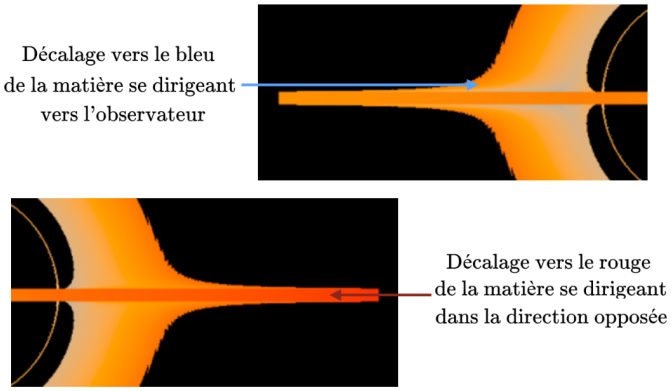

Fig. 17 Highlighting the Doppler-Fizeau effect near the plane of the disk

4.3 Einstein Shift

The last physical phenomenon that we propose to implement in our simulation is the Einstein shift or gravitational redshift. This effect originates from time dilation in the Schwarzschild geometry and is therefore based on purely relativistic reasoning. As in part 1, we admit the expression of the Schwarzschild metric. In geometric units, it is

written as:

$$ds^2 = -(1 - \frac{2M}{r})dt^2 + (1 - \frac{2M}{r})^{-1}dr^2 + r^2 d\theta^2 + r^2 \sin^2\theta d\phi^2$$

We also define the proper time linked to a Galilean reference frame by

$$d\tau^2 = -ds^2$$

(geometric unit). This is the time "experienced" by an observer inside such a reference frame. We consider a source of light wave located at a distance $r_{emitted}$ from the black hole that emits a wave assumed to be periodic with an "absolute" period, i.e., for an observer located at infinity, Δt. The clock associated with a stationary reference frame linked to the source measures the period of this wave in this reference frame, denoted $\Delta\tau_{emitted}$. The wave propagating at the speed of light c, in geometric units, the associated wavelength is rewritten as:

$$\lambda_{emitted} = c \times \Delta\tau_{emitted} = \Delta\tau_{emitted}$$

An observer is then located at a distance $r_{received}$ from the black hole in a reference frame assumed to be fixed. The clock associated with this reference frame measures the period of the wave denoted $\Delta\tau_{received}$. Similarly, $\lambda_{received} = \Delta\tau_{received}$. Now, the expression of the metric for a stationary reference frame becomes:

$$\Delta s^2 = -(1 - \frac{2M}{r})\Delta t^2 = -\Delta\tau^2$$

We deduce that, for the source and the observer:

$$\lambda_{emitted} = \sqrt{1 - \frac{2M}{r_{emitted}}}\Delta t$$

$$\lambda_{received} = \sqrt{1 - \frac{2M}{r_{received}}}\Delta t$$

Thus,

$$\lambda_{received} = \lambda_{emitted}\sqrt{\frac{1 - 2M/r_{received}}{1 - 2M/r_{emitted}}}$$

And since $r_R > r_{emitted}$, $\sqrt{\frac{1-2M/r_{received}}{1-2M/r_{emitted}}} > 1$ The light is therefore redshifted.

4.4 Simulation with the Addition of Gravitational Redshift

The gravitational redshift is implemented in the simulation in geometric units, as previously. We choose the same distance from the black hole as that used for the previous simulations. The result of a simulation on an image of resolution 1024×1024 pixels for

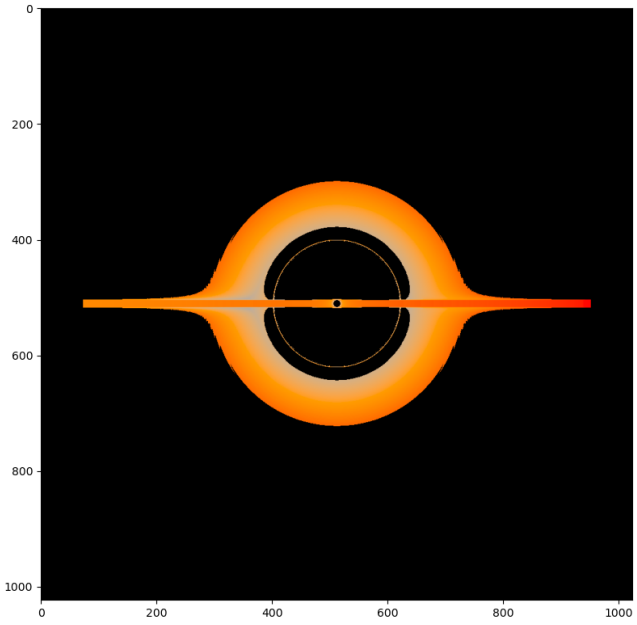

Fig. 18 Simulation of the observation of the black hole and its accretion disk with Einstein shift

which all the previously discussed physical phenomena are taken into account is presented in figure 18. Comments: The implementation of this last effect does not have a particularly notable effect. The stable orbits closest to the black hole have undergone a slight redshift but this is not considerably visible. This simulation nevertheless takes into account all the effects previously studied. It is the first illustration of the final model of the black hole and its disk. The following parts no longer aim to add new phenomena to the model but to bring better precision to the simulation.

4.5 Final Corrections

The numerical resolution method adopted in this project is an explicit first-order Euler method. It considerably reduces the computation time of the simulation but sometimes leads to approximations that are relatively imprecise compared to those of other numerical resolution methods. We have already mentioned in part 1 an aberration due to the resolution step chosen in the first-order Euler method, namely the "central circle" inside the disk represented in figure 19 and which has no physical reality. To remedy this aberration, we divide the resolution step of the simulation by 10. Moreover, for the last simulation, we increase the image size to 2048×2048 pixels. It is presented in figures 20 and 21. Comments: We note that by reducing the resolution step of the simulation, the "central circle" disappears. The choice of the simulation step was therefore indeed the cause of this aberration. Moreover, we can note that a second "halo" of photons seems to be drawn around the horizon and closer to it. The photons constituting this halo have probably made several orbits around the black hole before arriving at the camera. These last figures constitute the final stage of the

Fig. 19 Highlighting the aberration due to the resolution step

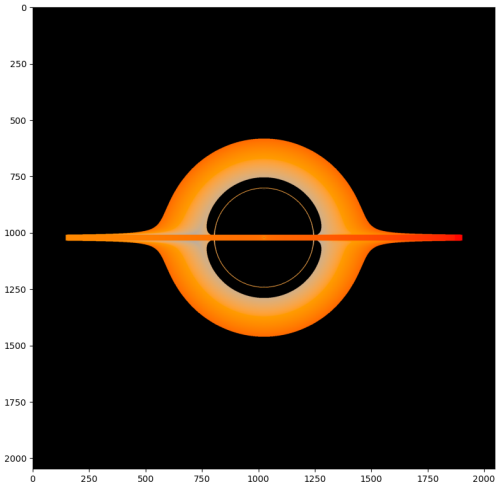

Fig. 20 Simulation of the observation of the black hole and its disk by reducing the simulation step by 10

simulation developed in this project: all the effects of photon deviation, color distribution, and frequency shifts come into play. As it stands, our simulation therefore provides a semi-realistic representation of a black hole and its accretion disk.

4.6 Discussion and Possible Improvements

Several aspects of the black hole and accretion disk model that we have developed during this project are debatable and could lead to improvements. • As previously discussed, the chosen numerical resolution method is the explicit first-order Euler method. Although this method was chosen for its speed of execution and ease of implementation, it can lead to inaccuracies and erroneous representation of objects. We could consider replacing it with a more costly but more precise numerical scheme, such as a fourth-order Runge-Kutta method. • In part 2, we modeled the radiation of the accretion disk as that of a black body. This hypothesis is relatively common for modeling the radiation of astrophysical objects such as stars. However, by converting the visible spectrum of a black body into RGB color, we do not represent the X-ray and gamma radiation that are nevertheless emitted in large quantities by real accretion disks [5]. We could imagine taking these phenomena into account and representing them in false color in parallel. • Although the modeling of the disk temperature, carried

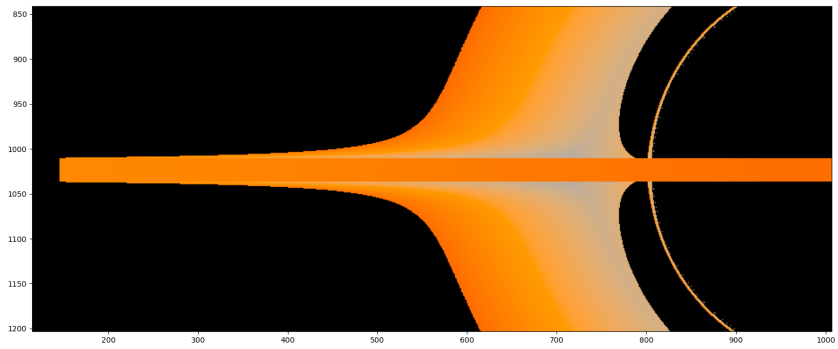

Fig. 21 Zoom on the last simulation

out in part 3, agreed with the $r^{-\frac{3}{4}}$ dependence of the Shakura and Sunyaev α disk model, the result was only valid up to a multiplicative constant, which had to be chosen arbitrarily for the simulation. For a more realistic representation, we could implement temperature distribution laws from more elaborate models such as that of Shakura and Sunyaev [5] or Novikov and Thorne [7]. There are currently many accretion disk models and it is still today a rich subject of research. • In addition to the temperature distribution, several other physical phenomena are involved in the realistic description of a real accretion disk, such as the magnetic forces involved, the turbulent flow of the "gas" in the disk, Compton diffusion, and radiation pressure due to radiation. A more advanced numerical simulation of the disk itself could involve these effects and describe the accretion disk in a more realistic way. • Finally, we chose for our model a Schwarzschild black hole, i.e., with zero angular momentum and charge. Although this choice allowed us to obtain simpler expressions to solve numerically, it could be considered to extend the study of photon deviation for a rotating black hole [8] (Kerr black hole) or charged (Reissner-Nordström or Kerr-Newman black hole).

5 Appendix

5.1 Last Stable Circular Orbit

In Newtonian celestial mechanics, it is always possible to find a stable circular orbit at any distance from the attracting body, provided that the right speed is given to the orbiting object. In general relativity, in the Schwarzschild metric, there is however a minimum radius below which it is impossible for a material object to have a stable orbit [2]. In the Schwarzschild metric, a material particle satisfies (in geometric units and with $\theta = \frac{\pi}{2} = cste$):

$$-1 = -(1 - \frac{2M}{r})(\frac{dt}{d\tau})^2 + (1 - \frac{2M}{r})^{-1}(\frac{dr}{d\tau})^2 + r^2(\frac{d\phi}{d\tau})^2$$

Hence, since $e = (1 - \frac{2M}{r})\frac{dt}{d\tau}$ and $l = r^2\frac{d\phi}{d\tau}$:

$$1 = (1 - \frac{2M}{r})^{-1}e^2 - (1 - \frac{2M}{r})^{-1}(\frac{dr}{d\tau})^2 - \frac{l^2}{r^2}$$

By multiplying the above by $(1 - \frac{2M}{r})$, we get:

$$(1 - \frac{2M}{r}) = e^2 - (\frac{dr}{d\tau})^2 - (1 - \frac{2M}{r})\frac{l^2}{r^2}$$

Hence, by rearranging the terms and dividing by 2:

$$\frac{1}{2}(\frac{dr}{d\tau})^2 - \frac{M}{r} + \frac{l^2}{2r^2} - \frac{Ml^2}{r^3} = \frac{1}{2}(e^2 - 1) = E$$

This expression can be interpreted as a conservation of energy E. We define, analogously to Newtonian mechanics, the effective potential:

$$V_{eff} = -\frac{M}{r} + \frac{l^2}{2r^2} - \frac{Ml^2}{r^3}$$

Thus, a stable circular orbit would satisfy: $\frac{dV_{eff}}{dr} = 0$ and $\frac{d^2V_{eff}}{dr^2} > 0$ That is:

$$\frac{dV_{eff}}{dr} = \frac{M}{r^2} - \frac{l^2}{r^3} + \frac{3Ml^2}{r^4} = 0$$

$$\frac{d^2V_{eff}}{dr^2} = -\frac{2M}{r^3} + \frac{3l^2}{r^4} - \frac{12Ml^2}{r^5} > 0$$

By multiplying the first equation by $\frac{2}{r}$ and summing the two expressions, we get:

$$\frac{l^2}{r^4} - \frac{6Ml^2}{r^5} > 0$$

That is: $r > 6M = r_{ISCO}$: this is the smallest stable circular orbit.

5.2 Demonstration of the Lorentz-Poincaré Transformation

We consider two Galilean reference frames $\mathcal{R}$ and $\mathcal{R}'$ in uniform rectilinear translation with respect to each other in the direction $Ox = Ox'$. We seek the relations between an event (x', y', z', t') seen in the reference frame $\mathcal{R}'$ and the same event (x, y, z, t) seen in the reference frame $\mathcal{R}$.

Postulate 1: We assume that the speed of light c in vacuum is invariant under change of Galilean reference frame. In a four-dimensional space, a uniform rectilinear motion is represented by a straight line. We therefore postulate that x, x' and t, t' are related by a linear relation of the form:

$$\begin{cases} x' = Ax \\ t' = Bt \end{cases}$$

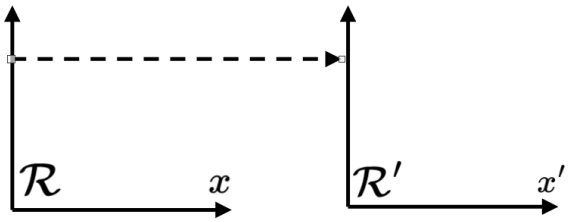

Fig. 22 Diagram of the situation

For an object moving at speed c in the direction of increasing x, according to postulate 1, the speed is the same in both reference frames, so:

$$\begin{cases} x = ct \\ x' = ct' \end{cases}$$

Thus, from the above,

$$x' - ct' = Ax - Bct = ct(A - B) = 0$$

This is true for all t so $A = B$ Thus, $x' - ct' = A(x - ct)$ Similarly, for an object moving at speed c in the direction of decreasing x, we obtain $x' + ct' = C(x + ct)$ (with C constant). By half-sum and half-difference of the previous equations, we obtain:

$$\begin{cases} x' = \frac{A+C}{2}x - \frac{A-C}{2}ct \\ ct' = \frac{A+C}{2}ct - \frac{A-C}{2}x \end{cases}$$

We denote $\gamma = \frac{A+C}{2}$ and $b = \frac{A-C}{2}$. We therefore seek to determine γ and b. We place ourselves at the origin of $\mathcal{R}'$: $x' = 0$ so $x = \frac{b}{\gamma}ct$ Now, $v = \frac{x}{t} = \frac{b}{a}c$ so $b = \frac{av}{c}$ The system then becomes:

$$\begin{cases} x' = \gamma(x - vt) \\ ct' = \gamma(ct - \frac{v}{c}t) \end{cases}$$

Postulate 2: (Principle of relativity) The expression of the laws of physics is the same in all Galilean reference frames. There is no privileged reference frame. The calculation carried out for $\mathcal{R}'$ moving at speed v with respect to $\mathcal{R}$ is also valid for the reference frame $\mathcal{R}$ moving at speed $-v$ with respect to $\mathcal{R}'$. Thus:

$$\begin{cases} x = \gamma(x' + vt') \\ ct = \gamma(ct' + \frac{v}{c}t') \end{cases}$$

Hence

$$x = \gamma(x' + vt') = \gamma(\gamma(x - vt) + \frac{v}{c}\gamma(ct - \frac{c}{c}x)) = \gamma^2(1 - \frac{v^2}{c^2})x$$

Thus, $\gamma^2(1 - \frac{v^2}{c^2}) = 1$ So

$$\gamma = \frac{1}{\sqrt{1 - \frac{v^2}{c^2}}}$$

Hence, since the translation is in the direction $Ox = Ox'$,

$$\begin{cases} x = \gamma(x' + vt') \\ ct = \gamma(ct' + \frac{v}{c}t') \\ y' = y \\ z' = z \end{cases}$$

We can rewrite this system in matrix form by noting $\beta = \frac{v}{c}$, we obtain:

$$\begin{pmatrix} ct \\ x \\ y \\ z \end{pmatrix} = \begin{pmatrix} \gamma & -\gamma\beta & 0 & 0 \\ -\gamma\beta & \gamma & 0 & 0 \\ 0 & 0 & 1 & 0 \\ 0 & 0 & 0 & 1 \end{pmatrix} \begin{pmatrix} ct' \\ x' \\ y' \\ z' \end{pmatrix}$$

This transformation remains true for any four-vector evolving like (ct, x, y, z) [6], which was the case in our study.

References

[1] Schwarzschild, K.: On the gravitational field of a mass point according to einstein's theory. Sitzungsber. Preuss. Akad. Wiss. Berlin (Math. Phys.) (1916) https://doi.org/10.48550/arXiv.physics/9905030

[2] Taillet, R., Moore, T.A.: Relativité Générale. Editions deboeck supérieur (2014)

[3] Guiselin, B.: Agrégation de chimie : Mécanique quantique. Cours de l'ENS Lyon années 2023-2024

[4] James, O., Tunzelmann, E.v., Franklin, P., Thorne, K.S.: Gravitational lensing by spinning black holes in astrophysics, and in the movie interstellar. Classical and Quantum Gravity 32 (2015) https://doi.org/10.48550/arXiv.1502.03808

[5] Shakura, N.I., Sunyaev, R.A.: Black holes in binary systems. observational appearance. Astronomy and Astrophysics (1973) https://doi.org/10.1007/978-94-010-2585-0_13

[6] Pérez, J.P.: Relativité et Invariance – Fondements et Applications. Editions Dunod, ISBN : 978-2100491735

[7] Page, D.N., Thorne, K.S.: Disk-accretion onto a black hole. time-averaged structure of accretion disk. The Astrophysical Journal (1974) https://doi.org/10.1086/152990

[8] Carter, B.: Global structure of the kerr family of gravitational fields. Phys. Rev. **174**, 1559–1571 (1968) https://doi.org/10.1103/PhysRev.174.1559